Atomic structure imaging of $L1_0$-type FePd nanoparticles by spherical aberration corrected high-resolution transmission electron microscopy

Kazuhisa Sato,[1,a)] Toyohiko J. Konno,[1] and Yoshihiko Hirotsu[2]
[1]*Institute for Materials Research, Tohoku University, Sendai 980-8577, Japan*
[2]*The Institute of Scientific and Industrial Research, Osaka University, Ibaraki 567-0047, Japan*

(Received 7 July 2008; accepted 18 December 2008; published online 9 February 2009)

The atomic structure of FePd nanoparticles has been studied by spherical aberration (C_s) corrected high-resolution transmission electron microscopy. The periodic arrangement of atoms arising from chemical order is clearly seen as bright contrast due to the small negative value of corrected C_s. The amount of optimal defocus (Scherzer defocus) is markedly reduced by the small C_s value. The interface between crystalline particles and the amorphous matrix can also be observed, free of imaging artifacts, at a small defocus value. The reconstructed phase image directly shows the projected potential distribution within the specimen and reveals the elemental differences due to chemical order. The clear-cut long-range order is lost when particle size is smaller than about 5 nm, at which locally ordered mixed-phase particles begin to dominate. © *2009 American Institute of Physics*. [DOI: 10.1063/1.3074505]

I. INTRODUCTION

The recent development of ultrahigh-density magnetic storage technology requires novel recording media with higher magnetocrystalline anisotropy energy, with the aims of increasing storage density and reducing recording noise. FePd nanoparticles with the $L1_0$-type ordered structure are good candidates for ultrahigh-density magnetic storage media.[1] The hard magnetic properties of these alloy nanoparticles are due to their tetragonal ordered structure with high magnetocrystalline anisotropy energy.[2] The evolution of the chemical order in FePd nanoparticles has been studied by high-resolution transmission electron microscopy (HRTEM) and electron diffraction,[3,4] while the size dependence of the long-range order has been examined by nanobeam electron diffraction.[5] However, the detailed atomic structure and a possible size limit of long-range atomic ordering are not yet understood.

Under normal HRTEM observation conditions, the finite spherical aberration of the objective lens requires a defocus value as large as 40–60 nm for optimal imaging, assuming a conventional high-resolution-type pole piece with a spherical aberration coefficient (C_s) of around 1 mm (Scherzer defocus, $\Delta f_{\mathrm{opt}}=\sqrt{\frac{4}{3}C_s\lambda}$, where λ is the electron wavelength).[6] Such a large defocus smears out fine details of phase contrast especially at the interface or defects of materials due to Fresnel fringes and contrast delocalization.[6] These wave-mechanical issues can be solved by correction of spherical aberration of the objective lens. In addition to highly improved spatial resolution, C_s-corrected TEM has the benefit of smaller defocus values under optimal defocus conditions due to small C_s values: for example, $\Delta f_{\mathrm{opt}}=8.9$ nm for $C_s=30$ μm, and even $\Delta f_{\mathrm{opt}}=1.6$ nm for $C_s=1$ μm. Hence, the optimal defocus of aberration-corrected TEM corresponds closely to the Gaussian focus, and this technique is now available.[7–9]

In this study, C_s-corrected TEM was used for high-resolution observation to determine the atomic structure of $L1_0$-FePd nanoparticles 2–10 nm in diameter, where the size effect has been shown to dominate the order-disorder transition.[10]

II. EXPERIMENTAL PROCEDURES

FePd alloy nanoparticles were fabricated by successive electron beam deposition of Pd and Fe onto NaCl(001) substrates at 673 K.[3,5] After deposition of Fe, an amorphous (a-)Al_2O_3 thin film was deposited to protect the particles from oxidation. The specimen film was then removed from the NaCl substrate by immersing the substrate into distilled water and was mounted onto conventional copper grids for TEM observation. Postdeposition annealing of the as-deposited film on a copper grid at 873 K for 3.6 ks led to the formation of the $L1_0$-type ordered structure in FePd nanoparticles.[3] The mean cooling rate was about 10 K/min. The orientation relationship between FePd and NaCl(001), as confirmed by electron diffraction, is $\langle 001\rangle_{\mathrm{FePd}}\|\langle 001\rangle_{\mathrm{NaCl}}$, $\{100\}_{\mathrm{FePd}}\|\{100\}_{\mathrm{NaCl}}$. The average alloy composition was Fe-49 at. % Pd according to the results of energy dispersive x-ray spectroscopy. HRTEM images were obtained using an FEI Titan 80-300 TEM operating at 300 kV with a field emission gun and a C_s-corrector for the objective lens. In this study, we adopted negative third-order spherical aberrations (C_{s3}) for HRTEM observation. All TEM images were recorded using a charge coupled device (CCD) camera attached to the TEM. HRTEM images were simulated based on the multislice method using the MACTEMPAS software. Focal-series HRTEM images were reconstructed using the TRUEIMAGE software package.

III. RESULTS AND DISCUSSION

Figure 1(a) shows a HRTEM image of a 10-nm-sized FePd nanoparticle with the c-axis of the $L1_0$ structure ori-

a)Electronic mail: ksato@imr.tohoku.ac.jp.

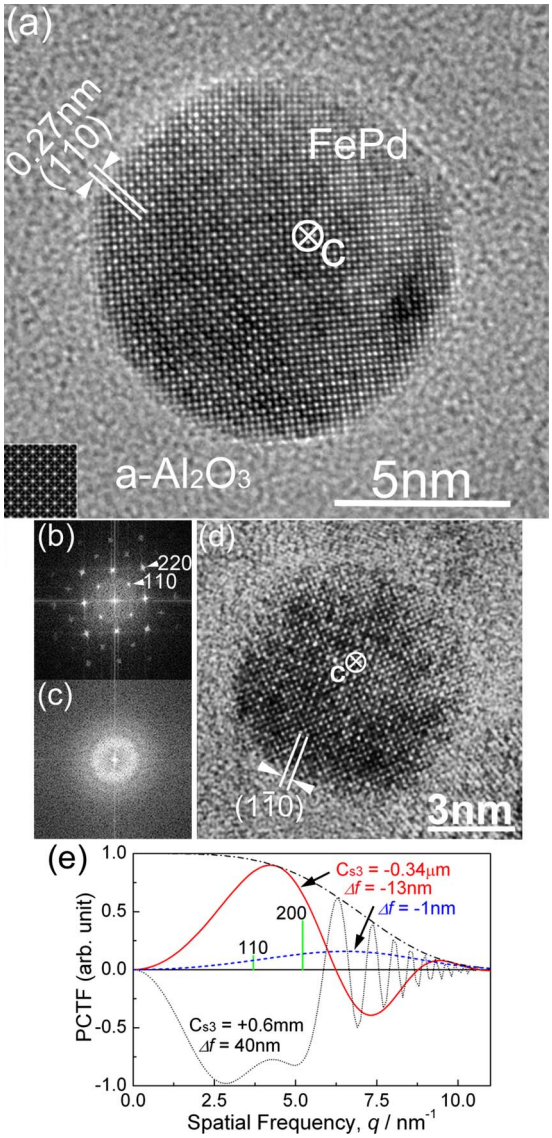

FIG. 1. (Color online) (a) HRTEM image of $L1_0$-FePd nanoparticle with the c-axis oriented normal to the film plane. The beam incidence is along $[001]_{FePd}$. The periodic arrangement of atoms by chemical order can be seen clearly. [(b) and (c)] Fourier spectra of nanocrystal and amorphous regions, respectively. The defocus was estimated to be −13 nm by analyzing the power spectra. (d) HRTEM image of $L1_0$-FePd nanoparticle observed with C_{s3}=0.6 mm for comparison. The PCTFs are shown in (e), where the solid curve shows the PCTF for the present experimental conditions. The PCTF for a typical conventional HRTEM with C_{s3}=0.6 mm is shown here for comparison (dotted line).

ented normal to the film plane, taken at C_{s3}=−0.34 μm. Clear {110} lattice fringes of the $L1_0$ structure can be seen in the nanoparticle. Due to the alternate stacking of Fe and Pd in the [001] direction in the $L1_0$ structure, the {220} atomic planes also possess an alternate stacking sequence of Fe and Pd in the ⟨110⟩ direction. This periodic stacking by chemical order causes intensity modulation at the atomic level. In addition, the arrangement of atoms due to chemical order can be seen unambiguously as periodic bright contrast in the HRTEM image even at the interface between the crystal and amorphous, as well as the inside of the nanoparticle. Figures 1(b) and 1(c) show Fourier spectra from the crystal and an amorphous region, respectively. Analysis of the power spectra in Fig. 1(c) indicated a defocus value of −13 nm (overfocus), which is slightly larger than the optimal defocus (Δf_{opt}=−1 nm) but much smaller than that for typical conventional HRTEM (Δf_{opt}=40 nm, C_{s3}=0.6 mm). An example of a conventional HRTEM image of an FePd nanoparticle taken with C_{s3}=0.6 mm is shown in Fig. 1(d) for comparison. This image was obtained using a JEOL JEM-3000F TEM operating at 300 kV with a field emission gun.[5] It should be noted that the atomic arrangement in the peripheral regions is not immediately obvious in Fig. 1(d) compared to the C_s-corrected image in Fig. 1(a), indicating that C_s correction is beneficial for imaging of nanoparticles. In the HRTEM observation under the weak phase object approximation (WPOA), the projected potential is modulated by the imaginary part of the transfer function sin $\chi(q)$. The phase contrast transfer function (PCTF), estimated for the present observation conditions, is shown as a solid line in Fig. 1(e). The PCTF is calculated using the following aberration function $[\chi(q)]$,[11,12] taking into consideration the fifth-order spherical aberration (C_{s5}=8 mm),

$$\chi(q) = -\pi\lambda\Delta f q^2 + \tfrac{1}{2}\pi C_{s3}\lambda^3 q^4 + \tfrac{1}{3}\pi C_{s5}\lambda^5 q^6, \qquad (1)$$

where q and Δf denote the scattering vector and the defocus, respectively. Here, a positive value of Δf signifies the underfocus condition. Note that the sign of the PCTF becomes positive when C_{s3} assumes a negative value, and hence the optimal defocus lies on the overfocus side, effectively compensating the focal deviation caused by the spherical aberration of the objective lens. The envelope function was estimated by Young's fringe test of the microscope, which indicated the information limit of q=10 nm^{-1} (corresponding to 0.1 nm resolution). For imaging, we used the criterion that the minimum of 5% of the PCTF should remain at the information limit below which the phase contrast is invisible.[13] The PCTF for the present experimental conditions has a large positive value and assumes a maximum at q=4.2 nm^{-1}, which is located between the spatial frequencies of 3.7 nm^{-1} (110 reflections) and 5.2 nm^{-1} (200 reflections). Under these conditions and with the WPOA, the projected potential is imaged as bright contrast. The inset of Fig. 1(a) is a simulated image, which also shows atom positions as bright contrast. The broken line in Fig. 1(e) indicates the PCTF at the optimal defocus for the present C_{s3} (Δf_{opt}=−1 nm). In this case, point resolution, defined by the first zero of the PCTF, corresponds to the information limit. In addition, the PCTF for a typical conventional HRTEM with C_{s3}=0.6 mm is shown here for comparison. Note that the PCTF for a small negative C_{s3} has a value slightly higher than that of the corresponding positive C_{s3} near the information limit. This is due to the asymmetry of the aberration function, i.e., the third term of Eq. (1) is always positive irrespective of the sign of C_{s3}.

Figure 2(a) shows a HRTEM image of an ordered FePd nanoparticle with its c-axis oriented parallel to the film plane. Periodic intensity modulation along the c-axis direction, with alternating bright and dark contrasts, is evident inside the whole nanoparticle. The Fourier spectrum in Fig. 2(b) shows spots, such as 001, arising from the periodic intensity modulation in the [001] direction. Separation of

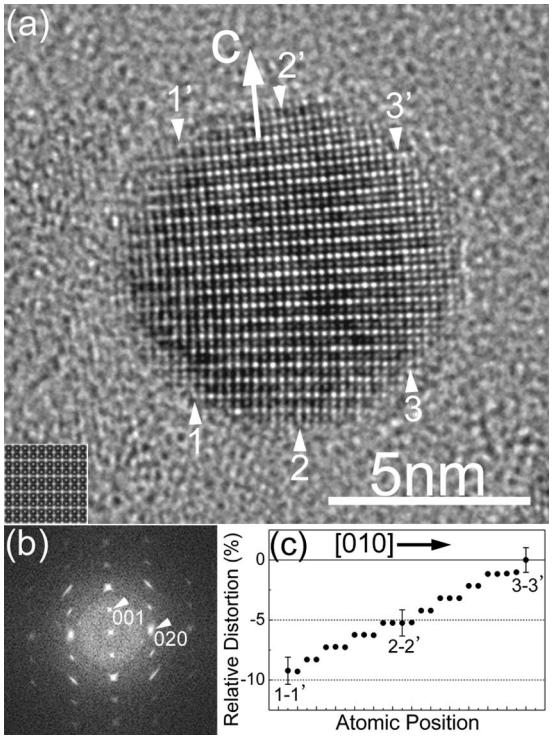

FIG. 2. (a) HRTEM image of $L1_0$-FePd nanoparticle with the *c*-axis oriented parallel to the film plane. The beam incidence is along $[100]_{FePd}$. (b) Fourier spectrum of the nanocrystal. (c) Relative distortion of (001) plane distance.

atomic rows, especially those due to (020) atomic planes in the [010] direction, is clear due to C_s correction compared to our previous results obtained by conventional HRTEM.[3] Also apparent in Fig. 2(a) is bending of the lattice image along the *c*-axis. Figure 2(c) summarizes the relative changes in the lattice spacing of (001) planes. The spacing was measured in the [001] direction and averaged over 10 unit cells, where the scale was calibrated using the lattice spacing of a nondistorted particle as the standard. The pixel size of the CCD camera gives error bars of ±1%, as indicated. It can be seen that (001) planes on the left-hand side of the particle are compressed with respect to those on the right-hand side. In fact, the amount of distortion varies linearly in the [010] direction, as shown in Fig. 2(c). For example, average (001) plane distance on lines 1-1′ and 2-2′ is distorted by −9.2% and −5.2%, respectively, relative to those on the line 3-3′. We examined over 100 particles and found that ~15% of nanoparticles, including those with the *c*-axis oriented normal to the film plane and those oriented parallel, exhibited similar distortion. One possible reason for the lattice distortion is compositional variation within a nanoparticle, as there are large differences between the atomic radii of Fe and Pd. In fact, surface segregation of Pt atoms in FePt nanoparticles with $L1_0$ structure was demonstrated by Yang *et al.*[14] using Monte Carlo simulation. However, their results suggested that only the very surface area is affected by Pt segregation, and therefore this is not the reason for the lattice distortion observed here. Enrichment of Pt atoms near the surface region of icosahedral nanoparticles of about 5–6 nm in diameter was also suggested by recent HRTEM observations.[15] In this case, however, icosahedral packing does not possess translational symmetry and already suffers from large strain. This is well known to be a structure that is unstable at large sizes, making it difficult to perform a direct comparison with the present findings regarding lattice distortion across the particle. Note that the clear intensity modulation along the *c*-axis shown in Fig. 2(a) indicates the alternate stacking of Fe and Pd in the [001] direction, which rules out inhomogeneous compositional variation as the origin of the lattice distortion. Another possible reason is strain distribution within the nanoparticle. Pan *et al.*[4] reported bending of lattice fringes in the periphery of disordered Fe–Pd nanoparticles embedded in MgO film. They offered an explanation based on the lattice mismatch between 0.21 nm of MgO(200) and 0.19 nm of FePd(200). Indeed, the Young's moduli of Fe and Pd are smaller than those of Al_2O_3 or MgO,[16] suggesting that the FePd nanoparticles can be easily deformed if they are constrained to the surrounding Al_2O_3 layer. In the present study, the bending of lattice fringes was observed only for particles smaller than 10 nm in diameter; however their appearance was not systematic: some of the particles were distorted, while others were not despite being the same size. Thus, it should not be concluded here that the observed distortion is due to a possible compositional variation or strain distribution. To elucidate the reasons for the distortion, further experiments, including size-dependent compositional analysis as well as *in situ* heating experiments, are necessary.

Figure 3 shows the phase of the exit-wave function by reconstructing a focal series of HRTEM images. A reconstructed phase image, in principle, excludes any effect of lens aberrations or defocusing.[17] In the reconstruction process, ten successive images were selected from the 20 focal series images, and the focal step analyzed *a posteriori* was 2 nm on average. In the phase image in Fig. 3(a), the particle periphery surrounded by the faceted interface can be seen clearly without contrast delocalization. In addition, Fig. 3(b), which is a magnified phase image, clearly resolves (220) atomic planes and the periodic arrangement of atoms by chemical order, corresponding to a resolution of 0.135 nm. The square indicates the unit cell of the ordered structure. Note that within the framework of WPOA, the contrast in the phase image corresponds directly to the projected electrostatic potential distribution within the specimen. Therefore, two types of bright dot, strong and weak, arise from the potentials of Pd and Fe atoms, respectively. Figure 3(c) shows an example of the intensity profile of the reconstructed phase image for both Fe and Pd rows, where solid and broken lines indicate intensity profiles of Pd and Fe rows, respectively, measured in the $[1\bar{1}0]$ direction. Symbols *X* and *X*′ correspond to the positions marked in Fig. 3(a), where the line *X*-*X*′ indicates a Pd row. At the central part of the particle, the intensity of the Pd atom column is higher than that of Fe by a factor of 40% at most, indicating the difference in projected atomic potentials between Pd and Fe. On the other hand, the intensity difference between Pd and Fe is not obvious at the peripheral region, which may indicate the possible variation in the chemical order close to the interface area. Thus, the reconstruction of phase images makes it possible to determine the elemental differences as well as clear-cut images of atomic rows.

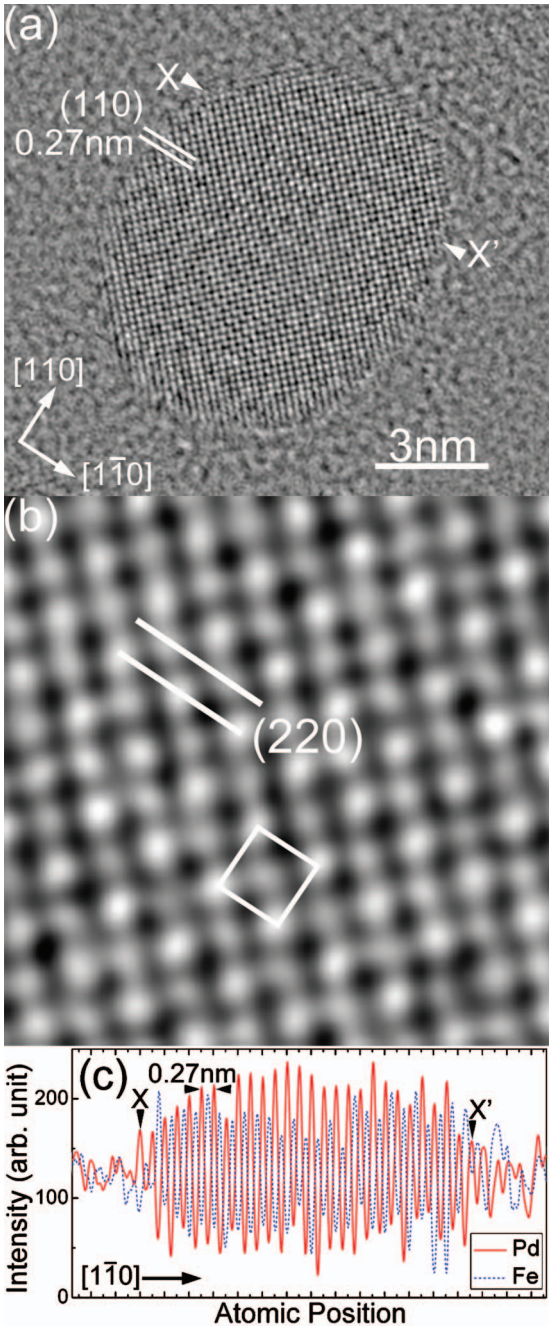

FIG. 3. (Color) (a) Phase image of exit wave reconstructed by focal series HRTEM images and (b) a magnified phase image of the chemically ordered region. Atomic distance of 0.135 nm, which corresponds to the (220) plane, can be seen clearly. The square indicates the unit cell of the ordered structure. (c) Intensity profiles for Pd (solid line) and Fe rows (broken line) measured in the [1$\bar{1}$0] direction on the phase image.

HRTEM images of the FePd nanoparticles of different sizes are shown in Fig. 4. All of these images were observed using small negative C_{s3} values under overfocus conditions. Atomic structures were clearly visualized even in very small FePd nanoparticles below 5 nm in diameter. It should be emphasized here that the image quality has been much improved by C_s correction compared to our previous study using conventional HRTEM.[18] It can be seen that when the particles are sufficiently large, the whole particle is ordered as indicated by (110) or (001) atomic plane with clear intensity modulation. In contrast, the particles are only locally ordered when the size is smaller than about 5 nm in diameter, as shown in Figs. 4(a)–4(d), which can also be recognized by faint superlattice reflections appearing in the corresponding Fourier spectra of these images (indicated by arrowheads). The smallest particle where the local ordering can be formed is 2 nm in diameter, as shown in Fig. 4(a). Note that local ordering means that only a limited part of a particle shows an ordered structure, while other parts of the particle are disordered. That is, the $L1_0$ ordered and the disordered fcc phases coexist in FePd nanoparticles smaller than 5 nm in diameter, although the $L1_0$ ordered structure is the stable structure of the bulk FePd alloy. This observation suggests that the instability of the ordered structure is caused by their small size with relatively large surface area.[19] This effect can be accounted for by the decrease in total energy difference between the ordered and the disordered states in nanoparticles.[20,21] According to the recent literature on FePt nanoparticles, which reported the stability of ordered phases based on experiment[22] and simulation,[14,23] the $L1_0$ structure with a high degree of order is formed even when the particles are as small as 3 nm in diameter, which differs significantly from the observations of FePd nanoparticles where the mixed phase is observed for particles below 5 nm in diameter. According to the equilibrium phase diagram,[24] the order-disorder transition temperature of FePt alloy is as high

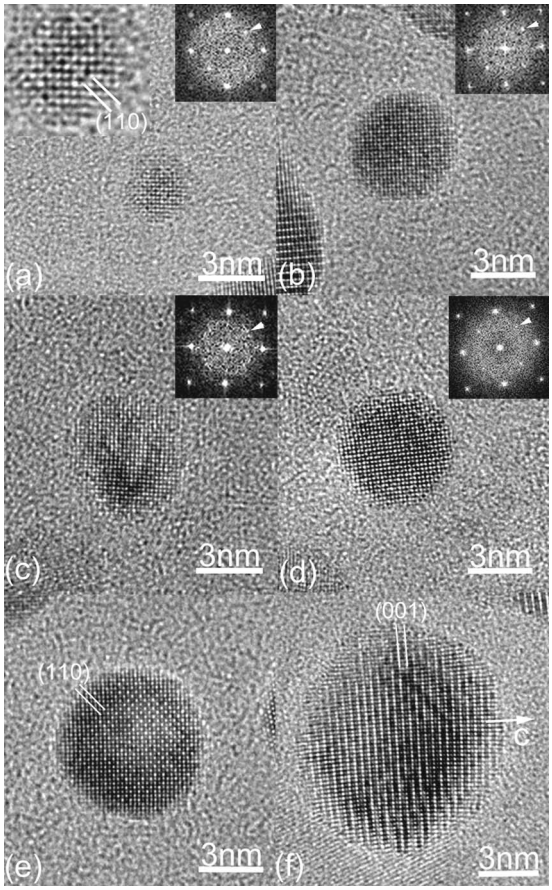

FIG. 4. HRTEM images of FePd nanoparticles showing the particle size dependence of atomic ordering. Particle diameters are (a) 2, (b) 4, (c) 5, (d) 5, (e) 6, and (f) 9 nm. The clear-cut long-range order is lost when particle size is smaller than about 5 nm in diameter.

as 1573 K, while that of FePd is 1063 K. This suggests that the free energy change upon ordering in FePt alloy is much larger than that of the FePd alloy, and this may be one of the reasons for the difference in size dependence of atomic ordering between FePd and FePt nanoparticles.

IV. SUMMARY

In conclusion, we demonstrated that the atomic structure of $L1_0$-FePd nanoparticles can be observed unambiguously by aberration-corrected HRTEM. The reconstructed phase image directly shows the projected potential distribution within the specimen. The periodic arrangement of atoms due to chemical order appears as bright contrast under conditions with a small negative C_{s3} value. The faceted particle interface can be imaged without contrast delocalization due to a small defocus, nearly corresponding to the Gaussian focus. The lattice bending and local chemical order inside a few nanometer-sized nanoparticles were also resolved in the present study. The clear-cut long-range order is lost when the size of particles is smaller than about 5 nm, and locally ordered mixed-phase particles become dominant, indicating the instability of the ordered FePd phase. It is therefore suggested that such a size effect is likely to place limits on industrial applications of small FePd nanoparticles.

ACKNOWLEDGMENTS

This study was partially supported by the Grant-in-Aid for Young Scientists (B) (Grant No. 19760459) and the Grant-in-Aid for Scientific Research (S) (No. 16106008) from the Ministry of Education, Culture, Sports, Science, and Technology, Japan. Electron microscopy was carried out in the High-Voltage Electron Microscope Laboratory, Tohoku University. The authors wish to thank Dr. K. Inoke of FEI Co. Japan Ltd., Mr. E. Aoyagi, and Mr. Y. Hayasaka of Tohoku University for their help using TEM.

[1] D. Weller and M. F. Doerner, Annu. Rev. Mater. Sci. **30**, 611 (2000).
[2] H. Shima, K. Oikawa, A. Fujita, K. Fukamichi, K. Ishida, and A. Sakuma, Phys. Rev. B **70**, 224408 (2004).
[3] K. Sato and Y. Hirotsu, J. Appl. Phys. **93**, 6291 (2003).
[4] H. Pan, S. Fukami, J. Yamasaki, and N. Tanaka, Mater. Trans. **44**, 2048 (2003).
[5] K. Sato, Y. Hirotsu, H. Mori, Z. Wang, and T. Hirayama, J. Appl. Phys. **98**, 024308 (2005).
[6] *High-Resolution Transmission Electron Microscopy and Associated Techniques*, edited by P. R. Buseck, J. M. Cowley, and L. Eyring (Oxford University Press, New York, 1992).
[7] S. Uhlemann and M. Haider, Ultramicroscopy **72**, 109 (1998).
[8] M. Haider, S. Uhlemann, E. Schwan, H. Rose, B. Kabius, and K. Urban, Nature (London) **392**, 768 (1998).
[9] M. Haider, H. Rose, S. Uhlemann, E. Schwan, B. Kabius, and K. Urban, Ultramicroscopy **75**, 53 (1998).
[10] K. Sato and Y. Hirotsu, Mater. Trans. **47**, 59 (2006).
[11] T. Hanai, M. Hibino, and S. Maruse, J. Electron Microsc. **33**, 329 (1984).
[12] A. Hirata, Y. Hirotsu, T. G. Nieh, T. Ohkubo, and N. Tanaka, Ultramicroscopy **107**, 116 (2007).
[13] M. Haider, H. Rose, S. Uhlemann, B. Kabius, and K. Urban, J. Electron Microsc. **47**, 395 (1998).
[14] B. Yang, M. Asta, O. N. Mryasov, T. J. Klemmer, and R. W. Chantrell, Acta Mater. **54**, 4201 (2006).
[15] R. M. Wang, O. Dmitrieva, M. Farle, G. Dumpich, H. Q. Ye, H. Poppa, R. Kilaas, and C. Kisielowski, Phys. Rev. Lett. **100**, 017205 (2008).
[16] M. F. Ashby and D. R. H. Jones, *Engineering Materials 1, An Introduction to Their Properties and Applications* (Pergamon, New York, 1987).
[17] A. Thust, W. M. J. Coene, M. Op de Beeck, and D. Van Dyck, Ultramicroscopy **64**, 211 (1996).
[18] Y. Hirotsu and K. Sato, J. Ceram. Proc. Res. **6**, 236 (2005).
[19] H. Numakura and T. Ichitsubo, Philos. Mag. **85**, 855 (2005).
[20] H. Yasuda and H. Mori, Z. Phys. D: At., Mol. Clusters **37**, 181 (1996).
[21] T. Tadaki, T. Kinoshita, Y. Nakata, T. Ohkubo, and Y. Hirotsu, Z. Phys. D: At., Mol. Clusters **40**, 493 (1997).
[22] T. Miyazaki, O. Kitakami, S. Okamoto, Y. Shimada, Z. Akase, Y. Murakami, D. Shindo, Y. K. Takahashi, and K. Hono, Phys. Rev. B **72**, 144419 (2005).
[23] R. V. Chepulskii and W. H. Butler, Phys. Rev. B **72**, 134205 (2005).
[24] *Binary Alloy Phase Diagrams*, 2nd ed., edited by T. B. Massalski, H. Okamoto, P. R. Subramanian, and L. Kacprzak (ASM International, Materials Park, OH, 1990).